Progress In Electromagnetics Research, PIER 16, 87–115, 1997

ANALYTICAL EVALUATION OF FINITE-DIFFERENCE TIME-DOMAIN TRANSMISSION LINE PROPERTIES

J. H. Oates

Sanders, A Lockheed Martin Company
Hudson, New Hampshire 03051, USA

R. T. Shin

Research Laboratory of Electronics
Massachusetts Institute of Technology
Cambridge, MA 02139, USA

1. INTRODUCTION

The Finite-Difference Time-Domain (FDTD) technique [1,2] has seen increasing application [3] in diverse topics of electromagnetic theory. The technique is simple to implement, can easily be applied to complex configurations, and provides accurate full-wave solutions over large frequency bands. One application that has been extensively researched is the modeling of transmission lines [3], and in particular, microstrip transmission lines and related microwave devices [4]. Microstrip lines find application in Microwave Integrated Circuits (MIC) and

Monolithic Microwave Integrated Circuits (MMIC) and in high-speed digital circuits. The FDTD technique has been used to model microstrip interconnects [5,6], vias [7], bends [8,9] and discontinuities in general [10].

An important parameter in the FDTD modeling of microstrip is the number of grid cells used to model the center strip conductor. Typically in transmission line modeling the grid cells are required to be smaller than $\lambda/10$, the limit imposed by dispersion, in order to capture the variation in the fields near the conductors. This is particularly true for microstrip, where the fields become infinite near the edge of the strip conductor. The number of grid cells that researchers have used to model the microstrip center conductor has typically been from six to eleven grid cells [4,9,11], although as few as four grid cells has been used [9]. Techniques have recently been presented for the subgrid modeling of microstrip lines in FDTD [12,13], which permits the microstrip line to be modeled in FDTD with fewer nodes.

When transmission lines are modeled in FDTD it is sometimes sufficient to use a transmission line with the same impedance and phase velocity as the actual transmission line being modeled. For example, in FDTD circular coaxial transmission lines are often modeled with rectangular coaxial structures. If the transmission line is used merely to connect different parts of a structure of interest, such as feeds to an antenna array, it may be desirable, if not necessary, to model the transmission lines with as few nodes as possible. For example, a single node spaced one cell above a ground plane may be used for a transmission line, provided the impedance and phase velocity are appropriate.

If a transmission line geometry is modeled with many nodes we can expect the fields and currents, and hence the impedance, to closely approximate those of the transmission line modeled. If, however, few nodes are used to model the line, then the FDTD line ceases to represent a real transmission line, as far as the fields and currents are concerned. Nevertheless these FDTD transmission lines propagate energy and have a definite impedance, and may be useful if the impedance can be found.

The purpose of this paper is to derive analytically the fields, currents and impedance of various open and closed FDTD transmission line geometries. Although the approach is applicable to transmission lines of arbitrary size, our focus is on geometries where the number of nodes used to model the lines are minimal, and hence the impedances

cannot be inferred from a corresponding continuum solution. The geometries examined include transmission lines modeled with a single node as the center conductor. The analytical techniques employed afford direct determination of FDTD transmission line parameters. For closed lines a set of linear equations are presented which determined the FDTD electric and magnetic fields. The voltage and currents, and hence the impedance, are determined from the electric and magnetic fields. It is also shown that the FDTD electric and magnetic fields can be determined directly from the solution of the finite difference equivalent of Laplace's equation on the FDTD grid.

For open lines such as microstrip, in addition to determining fields, currents, and impedance, the analytical solution gives the effective strip conductor width. The effective strip width of microstrip lines in FDTD is found by comparing the FDTD and continuum impedances. The heuristic approach models a strip of width w using w/Δ grid cells and $w/\Delta+1$ nodes [4,8,10,14], where Δ is the grid spacing. This corresponds to assuming the width of the strip conductor to end at the last node where the tangential electric field is forced to zero. There is, however, uncertainty in the actual width being modeled, particularly since, in general, we expect the FDTD and continuum results to differ where the corresponding continuum fields become infinite [15,16], such as at the edge of a microstrip conductor. It is shown that the actual width of an FDTD microstrip transmission line is approximately $w = (n - .25)\Delta$, where n is the number of nodes used to model the center conductor. This width is three quarters of a grid cell greater than the heuristic width, $w = (n - 1)\Delta$. The geometries examined include microstrip transmission lines modeled with as few as two nodes as the center conductor. For such cases determining the effective strip width accurately is particularly critical.

The analytical solution follows from the solution to TEM waves in FDTD. We begin in section 2 with an analysis of TEM wave propagation in FDTD, from which we determine the dispersion and impedance relations. In section 3 we consider closed transmission lines, determining analytically the impedances of various geometries. In section 4 we look at analytical solutions for open transmission lines such as twin lead and microstrip lines. In section 5 the analytically determined FDTD impedances are verified numerically.

2. TEM WAVE PROPAGATION IN FDTD

In this section we analytically solve the FDTD equations for TEM wave propagation, from which we derive the general dispersion and impedance relations for TEM waves in FDTD. In the following two sections these relations are used to determine the impedance of several closed and open transmission line geometries.

The FDTD equations in three dimensions, for the unit cell shown in Figure 1, are

$$e_x^p(l,m,n) = e_x^{p-1}(l,m,n) + \frac{\Delta\tau}{\epsilon_r\Delta}[h_z^{p-1}(l,m,n) - h_z^{p-1}(l,m-1,n) + h_y^{p-1}(l,m,n-1) - h_y^{p-1}(l,m,n)] \quad (1)$$

$$e_y^p(l,m,n) = e_y^{p-1}(l,m,n) + \frac{\Delta\tau}{\epsilon_r\Delta}[h_z^{p-1}(l-1,m,n) - h_z^{p-1}(l,m,n) + h_x^{p-1}(l,m,n) - h_x^{p-1}(l,m,n-1)] \quad (2)$$

$$e_z^p(l,m,n) = e_z^{p-1}(l,m,n) + \frac{\Delta\tau}{\epsilon_r\Delta}[h_y^{p-1}(l,m,n) - h_y^{p-1}(l-1,m,n) + h_x^{p-1}(l,m-1,n) - h_x^{p-1}(l,m,n)] - \frac{\Delta\tau}{\epsilon_r\Delta^2}\eta_0 I_z^p(l,m,n) \quad (3)$$

$$h_x^p(l,m,n) = h_x^{p-1}(l,m,n) - \frac{\Delta\tau}{\mu_r\Delta}[e_y^p(l,m,n) - e_y^p(l,m,n+1) + e_z^p(l,m+1,n) - e_z^p(l,m,n)] \quad (4)$$

$$h_y^p(l,m,n) = h_y^{p-1}(l,m,n) - \frac{\Delta\tau}{\mu_r\Delta}[e_x^p(l,m,n+1) - e_x^p(l,m,n) + e_z^p(l,m,n) - e_z^p(l+1,m,n)] \quad (5)$$

$$h_z^p(l,m,n) = h_z^{p-1}(l,m,n) - \frac{\Delta\tau}{\mu_r\Delta}[e_x^p(l,m,n) - e_x^p(l,m+1,n) + e_y^p(l+1,m,n) - e_y^p(l,m,n)] \quad (6)$$

where ϵ_r and μ_r are the relative dielectric constant and permeability respectively, Δ is the grid cell length, and $\Delta\tau = c\Delta t$ is the normalized time step. In the above, the indices (l,m,n) represent the spatial position and the superscript p the time step. The electric and magnetic field normalizations are $e_i \equiv E_i$ and $h_i \equiv \eta_o H_i$, where η_o is the free space impedance. A z-directed electric current $I_z^p(l,m,n)$ has been included in equation (3).

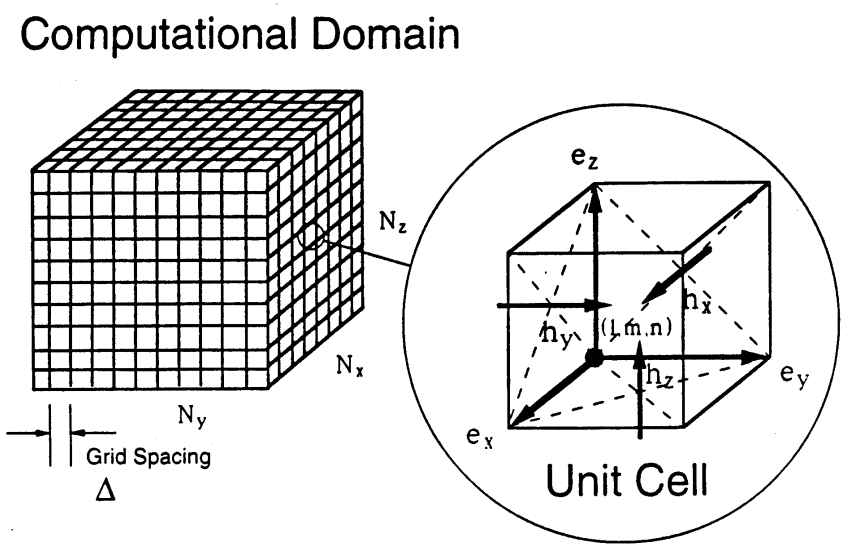

Figure 1. The computational domain and unit cell in the three dimensional implementation of the FDTD technique.

We seek TEM to z solutions of the FDTD equations, for which $e_z = h_z = 0$. For TEM to z solutions the FDTD equations become

$$e_x^p(l,m,n) = e_x^{p-1}(l,m,n) + \frac{\Delta\tau}{\epsilon_r \Delta}[h_y^{p-1}(l,m,n-1) - h_y^{p-1}(l,m,n)] \tag{7}$$

$$e_y^p(l,m,n) = e_y^{p-1}(l,m,n) + \frac{\Delta\tau}{\epsilon_r \Delta}[h_x^{p-1}(l,m,n) - h_x^{p-1}(l,m,n-1)] \tag{8}$$

$$h_x^p(l,m,n) = h_x^{p-1}(l,m,n) - \frac{\Delta\tau}{\mu_r \Delta}[e_y^p(l,m,n) - e_y^p(l,m,n+1)] \tag{9}$$

$$h_y^p(l,m,n) = h_y^{p-1}(l,m,n) - \frac{\Delta\tau}{\mu_r \Delta}[e_x^p(l,m,n+1) - e_x^p(l,m,n)] \tag{10}$$

Assuming each field component propagates as $e^{-ikp\Delta\tau + i\beta n\Delta}$ gives the dispersion and wave impedance relations

$$\sin(\beta\Delta/2) = \sqrt{\epsilon_r \mu_r}\frac{\Delta}{\Delta\tau}|\sin(k\Delta\tau/2)| \tag{11}$$

$$\eta_r h_x^p(l,m,n) = -e^{-ik\Delta\tau/2+i\beta\Delta/2} \cdot e_y^p(l,m,n) \tag{12}$$

$$\eta_r h_y^p(l,m,n) = e^{-ik\Delta\tau/2+i\beta\Delta/2} \cdot e_x^p(l,m,n) \tag{13}$$

where $\eta_r = \sqrt{\mu_r/\epsilon_r}$. The exponential factors $e^{-ik\Delta\tau/2+i\beta\Delta/2}$ reflect the offset in time and space between the electric and magnetic fields in FDTD.

The impedance relations give the characteristic impedance for TEM waves in FDTD. From the characteristic impedance, the transmission line impedance for a given geometry can be determined. In the next two sections the characteristic impedance for several closed and open transmission lines is determined. Henceforth we consider only cases for which $\epsilon_r = \mu_r = \eta_r = 1$.

3. ANALYTICAL SOLUTION FOR CLOSED TRANSMISSION LINES

In this section we analytically solve the FDTD equations for the impedance of several closed transmission line geometries. The analytical solutions follow from the FDTD impedance relations for TEM wave propagation developed in the previous section.

The FDTD transmission line impedance is $Z_{FDTD} = V/I$, where the voltage and currents on the TEM line are defined

$$V \equiv \int_P \overline{E} \cdot \overline{dl} \tag{14}$$

$$I \equiv \oint_C \overline{H} \cdot \overline{dl} \tag{15}$$

The integration path P for the voltage is any path in the transverse plane of the transmission line which connects the center conductor to the outer, or grounded, conductor. The circuit C for the current is any closed path in the transverse plane which encircles the center conductor.

For simple geometries like those shown in Figures 2 and 3 the impedance can be found by inspection. The geometry of Figure 2 employs a single node for the center conductor, whereas that of Figure 3 employs four nodes. By symmetry, for both geometries, all electric and magnetic field components are equal. Denoting the electric field components e and the magnetic field components h, we find for the

geometry in Figure 2

$$Z_{FDTD} = \frac{V}{I} = \frac{e\Delta}{4\Delta h/\eta_o} = \frac{1}{4}\eta_o \tag{16}$$

$$= 94.2\Omega \tag{17}$$

and for the geometry in Figure 3

$$Z_{FDTD} = \frac{V}{I} = \frac{e\Delta}{8\Delta h/\eta_o} = \frac{1}{8}\eta_o \tag{18}$$

$$= 47.1\Omega \tag{19}$$

where we have used $e/h = 1$, which negates the space and time displacements in the definition of the field components. Alternatively, we can take $e/h = e^{ik\Delta\tau/2 - i\beta\Delta/2}$ and define the impedance as

$$Z_{FDTD} \equiv e^{-ik\Delta\tau/2 + i\beta\Delta/2} \cdot \frac{V}{I} \tag{20}$$

which similarly accounts for the space and time displacements in the definition of the voltage and current. In [17] the impedance is defined as

$$Z_o \equiv \frac{V_n(\omega)e^{-ik\Delta\tau/2}}{\sqrt{I_{n-1}(\omega)I_n(\omega)}} \tag{21}$$

where $V_n(\omega)$ and $I_n(\omega)$ are respectively the frequency-domain voltage and current at node n. For time-harmonic fields the TEM frequency-domain voltage and current waves are

$$V_n(\omega) = V_o e^{i\beta n\Delta} \tag{22}$$

$$I_n(\omega) = I_o e^{-ik\Delta\tau/2 + i\beta(n+\frac{1}{2})\Delta} \tag{23}$$

where V_o and I_o are respectively the peak voltage and peak current along the line. Using the above expressions gives the impedance as

$$Z_o \equiv \frac{V_n(\omega)e^{-ik\Delta\tau/2}}{\sqrt{I_{n-1}(\omega)I_n(\omega)}} = e^{-ik\Delta\tau/2 + i\beta\Delta/2}\frac{V_n(\omega)}{I_n(\omega)} = \frac{V_o}{I_o} \tag{24}$$

Hence definitions (20) and (21) are identical and are equivalent to defining the impedance as the ratio of the peak voltage to peak current along the line.

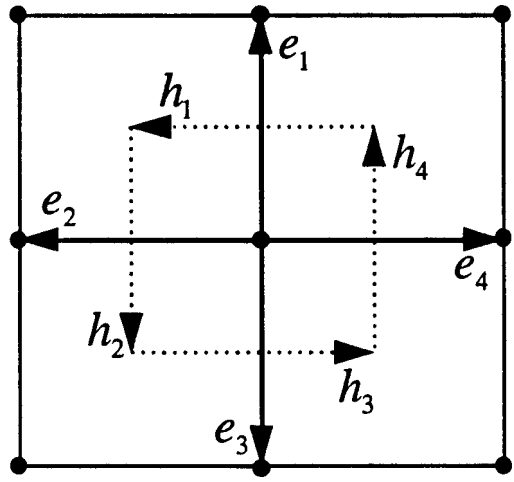

Figure 2. Closed transmission line with a single node for the center conductor. This is the smallest achievable FDTD transmission line. By symmetry all fields are equal. The impedance is $Z_o = \eta_o/4 = 94.2\Omega$.

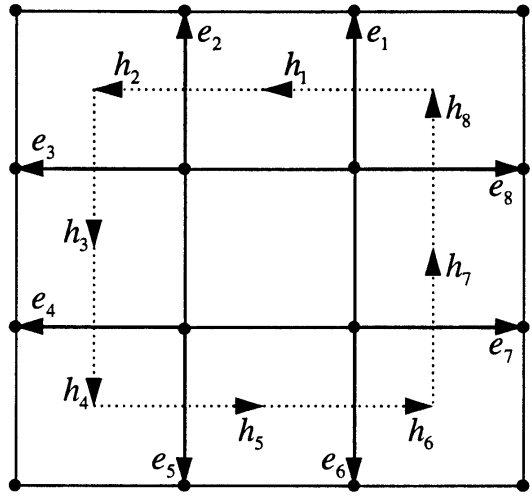

Figure 3. Closed transmission line with four nodes representing the center conductor. By symmetry all fields are equal. The impedance is $Z_o = \eta_o/8 = 47.1\Omega$.

For more complex geometries a set of simultaneous equations can be derived which determine the FDTD fields. Consider the geometry shown in Figure 4. Since there are no longitudinal (z-directed) fields, we have

$$\oint_C \overline{E} \cdot \overline{dl} = 0 \tag{25}$$

where C represents any circuit in the transverse plane. For circuit C_1 in Figure 5, for example, we find

$$e_3 - e_5 - e_1 = 0 \tag{26}$$

In addition to Equation (25) for circuits, there is an additional requirement which must be satisfied at nodes. For any node not at a conductor surface, there is no charge and hence

$$\nabla \cdot \overline{E} = 0 \tag{27}$$

For node n_2, for example, in Figure 5 we find

$$e_6 - e_5 + e_4 - e_3 = 0 \tag{28}$$

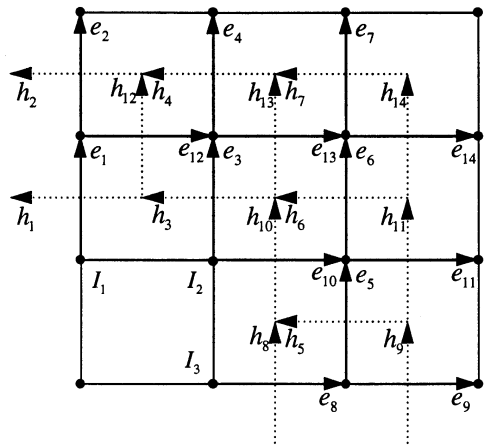

Figure 4. Closed transmission line with eight nodes representing the center conductor. The impedance is $Z_o = 6\eta_o/41 = 55.2\Omega$. Shown is the first quadrant of the geometry. The currents are $I_1 = I_3 = \Delta/\eta_o$ and $I_2 = 28\Delta/13\eta_o$.

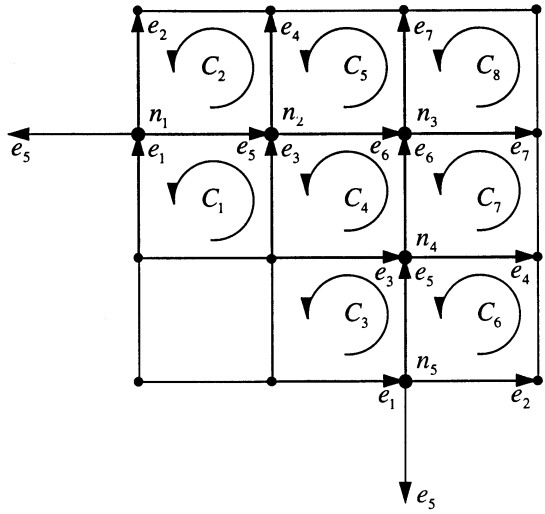

Figure 5. Closed transmission line geometry of Figure 4, showing the circuits C_i and nodes n_i. The x-directed electric field components are related to the y-directed field components due to symmetry.

This finite difference equivalent of Equation (27) is exact, following directly from the FDTD algorithm. Equation (27) is equivalent to

$$\oint_{C'} \overline{H} \cdot \overline{dl} = 0 \tag{29}$$

which is evident from the impedance relations $e_i = h_i$. This similarly only holds away from conductor surfaces, where there is no current.

In Figure 5 symmetry has been employed to determine the x-directed electric fields in terms of the y-directed fields. *Network Graph Theory* [18] can be used to develop a systematic approach to determining the set of sparse linear equations directly from the geometry. For the simple geometries considered here, however, the linear equations are easily determined.

For the geometry given in Figure 5, for example, there are eight circuits and five nodes on which to apply Equations (25) and (27), respectively. However, due to the symmetry of the problem, only circuits C_1, C_2, C_5 and nodes n_1, n_2, n_3 are unique, giving six equations in seven unknowns. The seventh equation comes from specifying the voltage. Alternately, however, we can arbitrarily set one of the field

components, which then determines the voltage. We choose the latter, setting $e_1 = 1$. The resulting solution to the system of equations is

$$\begin{aligned} e_1 &= 13/13 \qquad e_5 = 1/13 \\ e_2 &= 11/13 \qquad e_6 = 5/13 \\ e_3 &= 14/13 \qquad e_7 = 5/13 \\ e_4 &= 10/13 \end{aligned} \tag{30}$$

The impedance for this geometry is then

$$Z_{FDTD} = \frac{V}{I} = \frac{6}{41}\eta_o \tag{31}$$

$$= 55.2\Omega \tag{32}$$

The current distribution is concentrated at the corners of the square center conductor as expected. The currents I_1, I_2 and I_3 defined in Figure 4 are found to be $I_1 = I_3 = \Delta/\eta_o$, $I_2 = 28\Delta/13\eta_o$.

For large geometries, as mentioned above, a systematic approach to determining a set of sparse linear equations can be employed. Alternately, however, the FDTD fields can be determined from the solution to the finite difference equivalent of Laplace's equation, which can be solved using sparse matrix techniques or iterative relaxation techniques. Since all longitudinal fields are zero, a potential function $\phi(l, m, n)$ can be defined at each node according to

$$\phi(l+1, m, n) = \phi(l, m, n) - e_x(l, m, n)\Delta \tag{33}$$

$$\phi(l, m+1, n) = \phi(l, m, n) - e_y(l, m, n)\Delta \tag{34}$$

Starting from an arbitrarily defined reference node, the potential can be determined throughout the computational domain in terms of the electric field through the above equations. Alternately, the potential can be solved for directly, and subsequently the electric fields determined from the potential solution. Applying the above definition for the potential and condition (27) for interior nodes we find

$$\begin{aligned} \phi(l, m, n) = \frac{1}{4}[&\phi(l+1, m, n) + \phi(l-1, m, n) \\ &+ \phi(l, m+1, n) + \phi(l, m-1, n)] \end{aligned} \tag{35}$$

which is the finite difference equivalent of Laplace's equation. A convenient approach to solving the above equation is to employ the Successive Over-Relaxation (SOR) iterative method [19], which gives the

potential $\phi^{p+1}(l,m,n)$ at iteration $p+1$ in terms of the potential $\phi^p(l,m,n)$ and the residual $\Gamma^p(l,m,n)$ at iteration p:

$$\Gamma^p(l,m,n) = \phi^p(l,m,n) - \frac{1}{4}[\phi^p(l+1,m,n) + \phi^p(l-1,m,n) + \phi^p(l,m+1,n) + \phi^p(l,m-1,n)] \quad (36)$$

$$\phi^{p+1}(l,m,n) = \phi^p(l,m,n) - \alpha\Gamma^p(l,m,n) \quad (37)$$

where $0 < \alpha < 2$ is a relaxation parameter. For over-relaxation, $1 < \alpha < 2$, which provides fast convergence.

The above transmission lines are closed geometries. In the next section we consider open transmission lines such as twin lead and microstrip transmission lines.

4. ANALYTICAL SOLUTION FOR OPEN TRANSMISSION LINES

We consider here open transmission lines such as single-wire, twin-lead and microstrip transmission lines. For open transmission lines the simple methods of the previous section cannot be used since that would result in an infinite number of equations. An analytical FDTD solution for TEM propagation along a wire can be used, however, as a Green's function, which can be used to solve for the impedance and current distribution for many different TEM open transmission line geometries.

For propagating TEM wave solutions to the FDTD algorithm the longitudinal components of the electric and magnetic fields are zero, and hence we require $e_z^p(l,m,n) = 0$ and $h_z^p(l,m,n) = 0$. We assume, in addition, a z-directed traveling-wave electric current

$$\eta_0 I_z^p(l,m,n) = \eta_0 I_o \delta_{ll_o} \delta_{mm_o} e^{-ikp\Delta\tau + i\beta n\Delta} \quad (38)$$

As for the closed transmission lines all field components propagate along the z-axis according to the exponential factor $e^{-ikp\Delta\tau+i\beta n\Delta}$. Given the above current and the TEM-wave constraint, the FDTD equations can be solved. The approach is similar to that employed in [20] for determining the fields of a line source. Initially a finite computational domain is assumed. All fields are expanded in terms of the Discrete Fourier Transform (DFT), through which the FDTD difference equations become algebraic equations. Once these transformed

fields are determined, the fields in the spatial domain are found from the Inverse DFT (IDFT). The computational domain is then extended to infinity, which gives the fields in terms of integrals over the first Brillouin zone of the reciprocal FDTD lattice. The details of the analytical FDTD solution under the above conditions are given in the appendix.

The approach outlined above yields the FDTD solution for a traveling TEM wave guided by a single wire in free space. The x-directed magnetic field solution is

$$h_x^p(l,m,n) = \frac{-\eta_0 I_o e^{-ik(p+1)\Delta\tau + i\beta n\Delta}}{4\pi} \cdot \int_{-\frac{\pi}{\Delta}}^{\frac{\pi}{\Delta}} dk_y \frac{\left|\sin[k_y(m-m_o+\frac{1}{2})\Delta]\right|}{\cos(k_{ox}\Delta/2)} e^{ik_{ox}|l-l_o|\Delta} \tag{39}$$

For parallel wire twin-lead tansmission lines, or equivalently, for a wire above a ground plane, as shown in Figure 6, we add the image solution giving

$$h_x^p(l,m,n) = \frac{\eta_0 I_o e^{-ik(p+1)\Delta\tau + i\beta n\Delta}}{2\pi} \cdot \int_{-\frac{\pi}{\Delta}}^{\frac{\pi}{\Delta}} dk_y \frac{|\sin[k_y m_o\Delta]|\cos[k_y(m+\frac{1}{2})\Delta]}{\sqrt{1+\sin^2(k_y\Delta/2)}} e^{ik_{ox}|l-l_o|\Delta} \tag{40}$$

The voltage induced by the impressed current is given as the integral of the electric field over the path indicated in Figure 6. Using the impedance relations for TEM waves gives the electric field

$$e_y^p(l,m,n) = \frac{-2\eta_0 I_z^p(l_o,m_o,n)}{\pi\Delta} e^{-ik\Delta\tau/2 - i\beta\Delta/2} \cdot \int_0^{\frac{\pi}{2}} dy \frac{\sin(2m_o y)\cos[(2m+1)y]}{\sqrt{1+\sin^2 y}} e^{i2u_{ox}|l-l_o|} \tag{41}$$

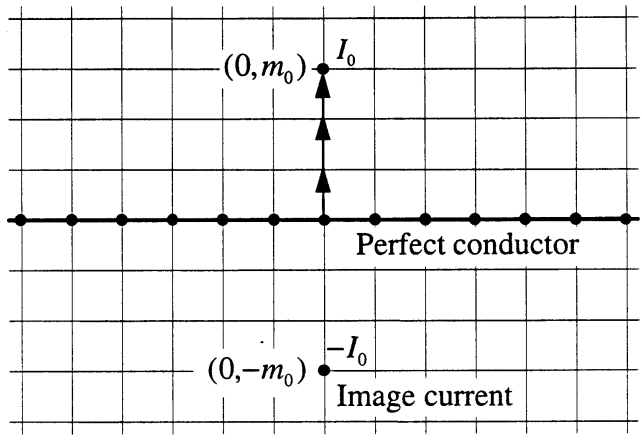

Figure 6. Geometry for a wire above a ground plane. A z-directed current I_o is located at point $(l,m) = (0,m_o)$. The solution for the FDTD fields for $m > 0$ is found by including an image current at the point $(l,m) = (0,-m_o)$. The path from $(0,0)$ to $(0,m_o)$ is the integration path for determining the voltage induced by the current I_o.

where the substitution $y = k_y\Delta/2$ has been made, and

$$\begin{aligned} u_{ox} &\equiv \frac{k_{ox}\Delta}{2} \\ &= i\mathrm{Ln}\left[\sin y + \sqrt{1+\sin^2 y}\right] \end{aligned} \tag{42}$$

The impedance is then given as

$$Z_o = \frac{-\Delta}{I_z^p(l_o,m_o,n)} \sum_{m=0}^{m_o-1} e_y^p(l_o,m,n) \tag{43}$$

$$= \frac{1}{\pi}\eta_0 \int_0^{\frac{\pi}{2}} dy \frac{\sin^2(2m_o y)}{\sin y\sqrt{1+\sin^2 y}} \tag{44}$$

where again we have neglected the exponential factor in keeping with our definition of the impedance in terms of peak fields. The impedance

m_0	$Z_0(\Omega)$	a/Δ
1	137.0	0.206
2	179.8	0.203
3	204.4	0.199
4	221.7	0.198
5	235.1	0.198

Table 1. Impedance and equivalent node radius for a transmission line consisting of a single node above a ground plane. The equivalent node radius is approximately independent of the height m_o.

of the corresponding continuum solution, that of a wire of radius a a distance h above a ground plane is,

$$Z_o = \frac{\eta_0}{2\pi} \mathrm{Ln}\left[\frac{h}{a} + \sqrt{\left(\frac{h}{a}\right)^2 - 1}\right] \tag{45}$$

In order to compare the FDTD and continuum solutions we need the equivalent radius, a, of a single node transmission line in FDTD. Alternately, we can equate the FDTD and continuum impedances and hence derive the equivalent FDTD radius of a single node. Table 1 shows the derived radius a for various heights $h = m_o\Delta$ found by equating the FDTD and continuum impedances. The results show that the effective radius for TEM waves is nearly $a/\Delta = 0.2$, which is approximately independent of the height m_o.

We now turn to the microstrip geometry. We consider only the case for which the substrate relative dielectric constant is $\epsilon_r = 1$ so that the TEM wave assumption remains exact. The microstrip line solution in FDTD can be determined by using multiple lines, each with a different current, where the current is determined so that the voltage is constant along the nodes representing the strip conductor. This is equivalent to enforcing zero tangential field along the conductor. The voltage V_l at $x = l\Delta$ for a single current at $x = l_o\Delta$, as shown in Figure 7 is

$$V_l = -\sum_{m=0}^{m_o-1} e_y^p(l, m, n)\Delta \tag{46}$$

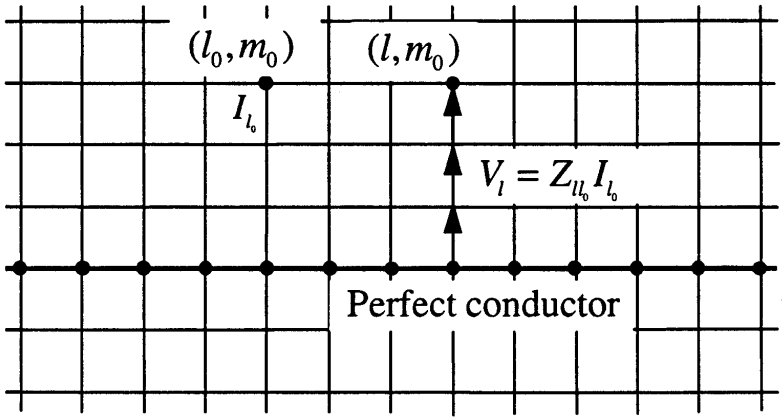

Figure 7. Shown is the voltage V_l at (l, m_o) induced by the current I_{l_o} at (l_o, m_o).

$$= \frac{\eta_0 I_{l_o}}{\pi} \int_0^{\frac{\pi}{2}} dy \frac{\sin^2(2m_o y)}{\sin y \sqrt{1+\sin^2 y}} \cdot \left[\sin y - \sqrt{1+\sin^2 y}\right]^{2|l-l_o|} \quad (47)$$

$$= Z_{ll_o} I_{l_o} \quad (48)$$

$$Z_{ll_o} \equiv \frac{\eta_0}{\pi} \int_0^{\frac{\pi}{2}} dy \frac{\sin^2(2m_o y)}{\sin y \sqrt{1+\sin^2 y}} \cdot \left[\sin y - \sqrt{1+\sin^2 y}\right]^{2|l-l_o|} \quad (49)$$

For a microstrip transmission line represented by multiple wires, as shown in Figure 8 the total voltage at $x = l\Delta$ is the sum of the voltages due to each wire:

$$V_l = \sum_{l_o=1}^{N} Z_{ll_o} I_{l_o} \quad (50)$$

The voltages V_l must be constant, independent of l. Setting $V_l = V_o$, a constant, gives us a set of linear equations for the microstrip currents I_{l_o}. Once the currents are determined, the impedance is the

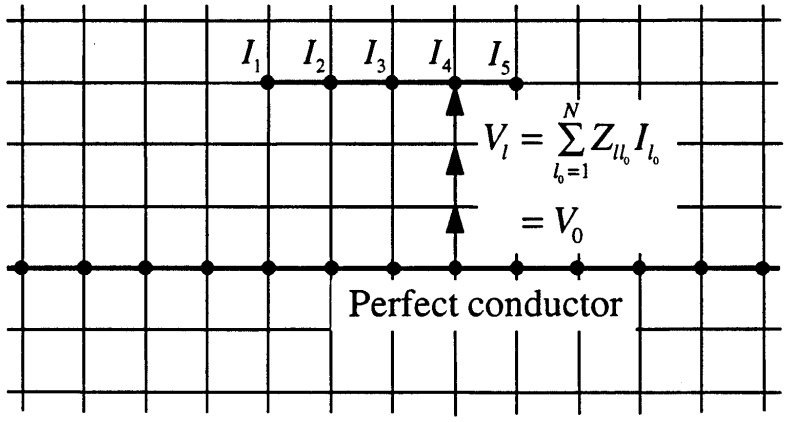

Figure 8. Geometry of a microstrip transmission line composed of $N = 5$ wires above a ground plane. The voltage V_l is the sum of the voltages induced by the currents I_{l_o}. Enforcing $V_l = V_o$, a constant independent of l, yields a set of N simultaneous equations for the currents I_{l_o}.

ratio of voltage to total current

$$Z_o = \frac{V_o}{\sum_{l_o=1}^{N} I_{l_o}} \tag{51}$$

Figure 9 shows the geometry for various FDTD microstrip transmission lines, and Table 2 shows the impedance and effective strip width for the geometries in Figure 9. The current distributions are shown in Figure 10. The effective strip width is found by equating the FDTD impedance with the corresponding continuum impedance.

The effective width is then [21]

$$w = 8h \frac{\sqrt{\exp(Z_o/30) - 1 + \pi^2/4}}{\exp(Z_o/30) - 1} \tag{52}$$

where $h = m_o\Delta$ is the height of the strip above the ground plane and Z_o is the FDTD microstrip impedance. The effective strip width is

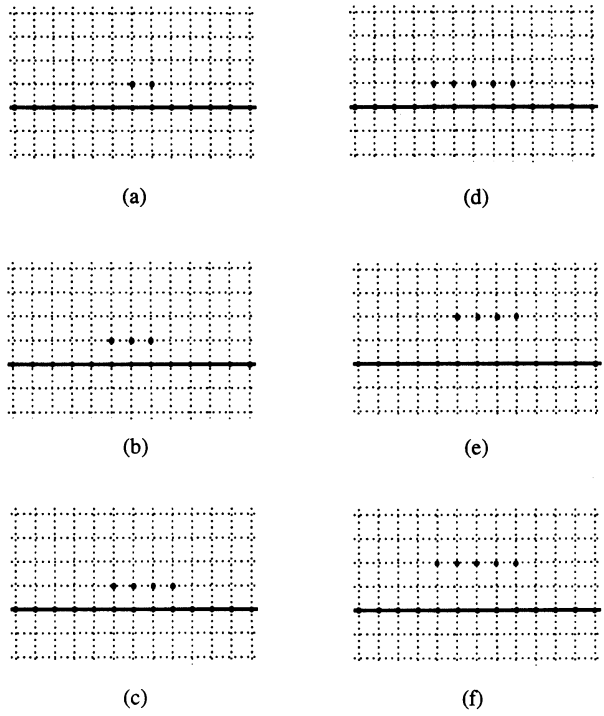

Figure 9. Various microstrip geometries. The effective strip width, w, is found to approximately follow $w = (n - .25)\Delta$, where n is the number of nodes representing the center conductor.

Geometry	$Z_0(\Omega)$	w/Δ
a	94.3	1.79
b	72.9	2.77
c	59.8	3.75
d	50.9	4.73
e	92.3	3.72
f	80.6	4.70

Table 2. Impedance and effective strip width for the microstrip transmission lines shown in Figure 9. The effective strip width is observed to follow approximately $w = (n - .25)\Delta$, where n is the number of nodes representing the strip conductor.

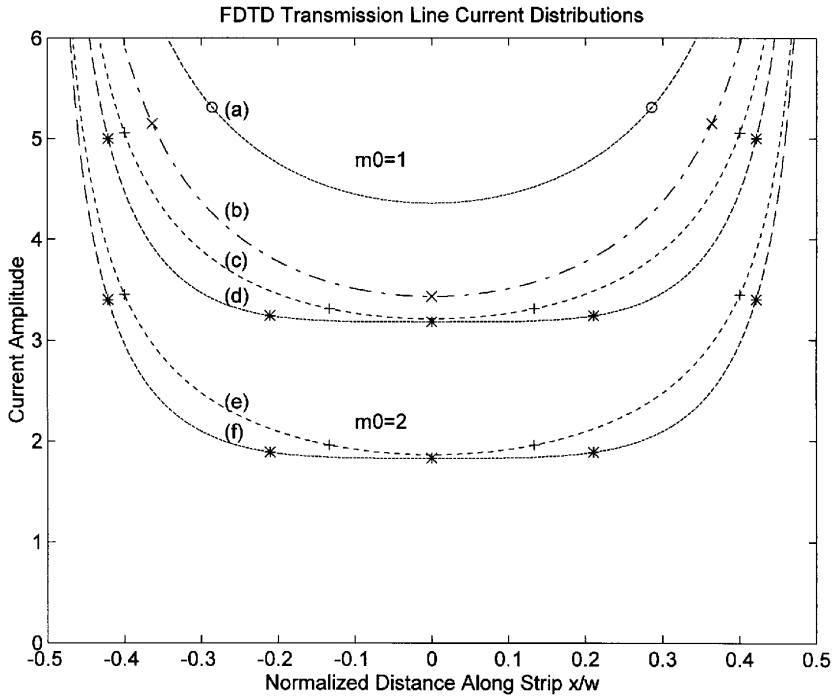

Figure 10. The current distributions for the various microstrip geometries shown in Figure 9. The height of the strip above the ground plane is $m_o\Delta$.

observed to follow approximately $w = (n - .25)\Delta$, where n is the number of nodes representing the strip conductor. Thus the FDTD effective strip width is three quarters of a grid cell greater than the heuristic width typically used in modeling microstrip lines in FDTD [4][8][10][14]. This represents on each side of the strip a $3\Delta/8$ extension of the conductor beyond the last node representing the strip, which is important when only a few nodes are used to model the microstrip line. Notice also that the current distributions shown in Figure 10 exhibit the characteristic microstrip edge effect.

Although our focus has been on transmission lines modeled with only a few nodes, the method, as mentioned above, is applicable to lines modeled with many nodes, and can be used for determining accurate impedance values of these lines. If the incorrect strip width is used to

determine the impedance large errors can result, even for lines modeled with many nodes. For example, if eight nodes are used to model a strip center conductor the resulting error in impedance due to using the heuristic width is 7.5%.

5. NUMERICAL VERIFICATION OF THE ANALYTICAL FDTD IMPEDANCE

We consider first the numerical verification of the closed transmission line impedances found in Section 3. Our objective is to verify the analytically determined impedances by applying the time-marching FDTD algorithm to the transmission line geometries of Figures 2, 3 and 4. We want to show that the impedance determined through the time-marching application of the FDTD algorithm yields the same solution as that determined analytically.

Our approach is to excite the transmission line such that only the dominant mode is present. By avoiding higher-order modes the impedance determination is more accurate, and is independent of where along the line the impedance is calculated. To launch a single mode we use the analytically determined field distribution, forcing the transverse fields at $n = 0$. At the end of the line we place a short circuit. The length of the transmission line is long enough so that reflected waves do not interfere with the results. The line is excited with a sinusoidal field, and the voltage and current is computed versus time at a point $n = n_m$ along the line. The peak voltage and current at $n = n_m$ are calculated using a quadratic curve fit to find the extrema in time. The impedance is calculated as the ratio of the peak voltage to peak current. Before calculating the impedance we wait for transients to decay. Several voltage and current maxima are used to compute a mean and standard deviation of the impedance.

Table 3 shows a comparison of the analytically and numerically determined transmission line impedances for the geometries of Figures 2, 3 and 4. The impedance and accuracy values given for the numerically determined impedances are found from the mean and standard deviation of the samples. The variation evident in the impedance is due to a number of inaccuracies, including high frequency transients and the random peak location in time relative to the time steps. The percentage error between the analytically and numerically determined impedances is less than 0.04%, and the results were found to be independent of where along the line the voltage and current were calculated.

Geometry	$Z_0(\Omega)$ Analytical	$Z_0(\Omega)$ Numerical
Figure 2	94.184	94.218 ± 0.086
Figure 3	47.092	47.109 ± 0.043
Figure 4	55.152	55.152 ± 0.050

Table 3. Comparison of analytically and numerically determined FDTD transmission line impedance.

The time-marching method used to verify closed lines is impractical for verifying open lines. We want to resolve the effective strip width w to within a fraction of a grid cell in order to verify that $w = (n - .25)\Delta$ is more accurate than $w = (n - 1)\Delta$, the heuristic width. For open lines absorbing boundary conditions must be used to terminate the computational domain. These are characteristically difficult to implement for open lines, and introduce reflections which degrade accuracy [10,11,14]. For this reason we choose to use a large computational domain terminated by a perfect conductor to approximate the open line. Since the outer conductor is at a large distance from the region of strong fields the additional capacitance introduced by the outer conductor is small [22,23].

A second difficulty with open lines is that it is difficult to excite a single mode. This is also true for the closed line approximation since the cross-section is large. Multimode excitation results in larger errors than single mode. Hence for open lines we abandon verification through application of the time-marching FDTD algorithm. Instead, we verify that the closed FDTD impedance approaches the open transmission line impedance as the outer conductor becomes increasingly distant. The geometry of the closed line approximation is shown in Figure 11.

Figure 12 shows the FDTD transmission line impedance for the closed geometry shown in Figure 11 for three center conductor configurations, corresponding to the open transmission line geometries (b), (d) and (f) shown in Figure 9, as a function of the height m_{max} of the computational domain. These geometries were chosen since symmetry can be employed to cut the computational domain in half by placing a magnetic wall at $l = 0$. The SOR method with $\alpha = 1.85$ was em-

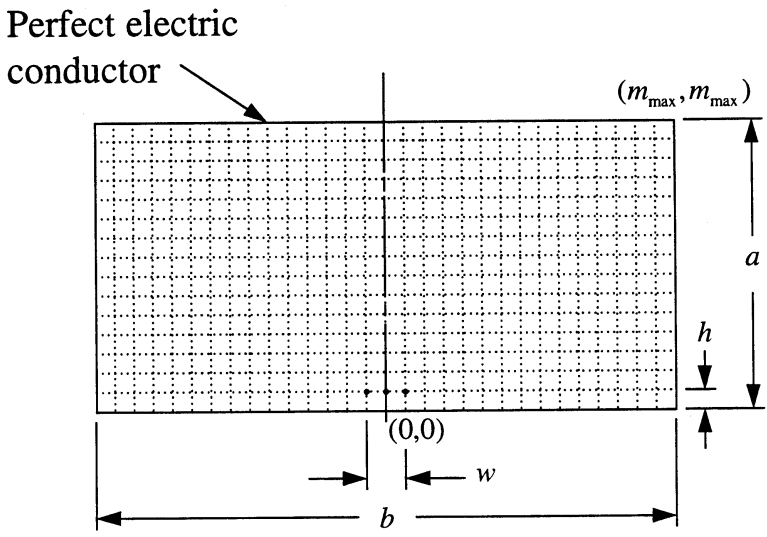

Figure 11. Geometry of a closed transmission line approximation to an open transmission line. The maximum extent of the computational domain, m_{max}, is taken to be very large to approximate an open transmission line.

ployed to compute the potential function from which the FDTD fields and impedance were evaluated. The iteration was continued until the maximum residual Γ_{max} satisfied $\Gamma_{max} < 1 \times 10^{-6}$. At each iteration the error $\Delta Z_o(t) \equiv |Z_o(t) - Z_o|$ where t is the iteration number, was bounded by equating

$$|dZ_o(t)/dt| = t^{-n} \tag{53}$$

from which the exponent n can be determined. It is observed that the exponent n slowly increases so that

$$\Delta Z_o < \frac{t_o^{1-n}}{(n-1)} \tag{54}$$

for $n > 1$, where t_o is the final iteration. The maximum error ΔZ_o in impedance, due to the iterative solution, for all cases considered was less than 0.043Ω.

For comparison purposes the closed impedance is compared in Figure 12 with the open transmission line impedance found from assuming

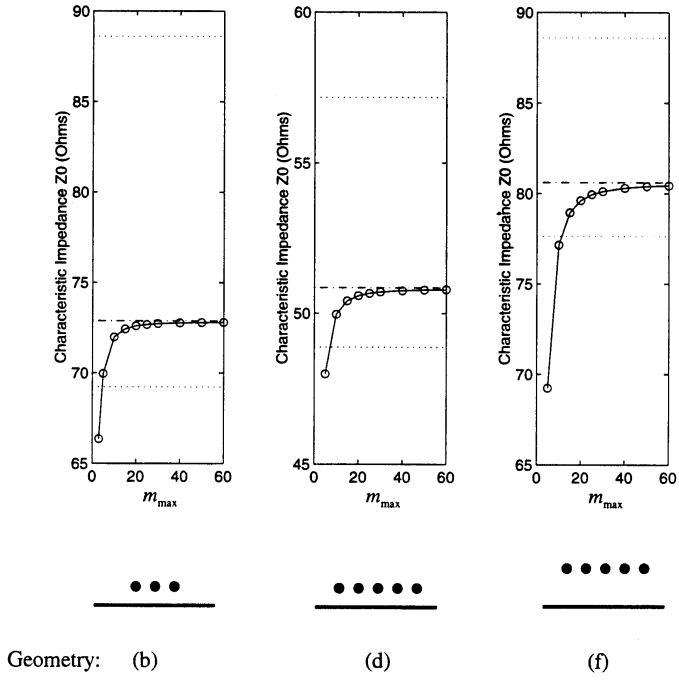

Figure 12. Comparison of the analytically determined FDTD open transmission line impedance (dot-dashed line) with the closed transmission line impedance for the line shown in Figure 11, which approximates the open line for large m_{max} . The dotted lines correspond to the microstrip impedances for strip widths $w = (n-1)\Delta$ and $w = n\Delta$.

an effective strip width $w = (n-1)\Delta$ and $w = n\Delta$ (dotted lines), and with the analytically determined open transmission line impedance (dot-dashed line). The closed transmission line impedance is observed to approach very closely the corresponding open transmission line impedance. As expected, the closed transmission line impedance is less than the open line impedance due to the additional capacitance introduced by the outer conductor. For geometry (f) the convergence is slower since the geometry is larger and hence the fields extend to greater distances.

6. CONCLUSIONS

In this paper we have presented an analytical derivation of the fields, currents and impedances of various FDTD transmission line geometries. The geometries considered were such that the number of nodes used to model the lines are minimal. The analytical solutions for TEM wave propagation in FDTD were presented, from which dispersion and impedance relations were determined. Both closed and open transmission lines were considered. For microstrip lines the analytically derived effective strip conductor width is found to be $w = (n - .25)\Delta$, which is three quarters of a grid cell greater than the heuristic width, $w = (n - 1)\Delta$. The results presented allow the impedance of FDTD lines to be computed from the closed-form impedance expressions of the corresponding continuum transmission lines. It has been shown that if the heuristic width is used to determine impedance large errors can result, even for lines modeled with many nodes. Both the closed and open transmission line impedances were verified numerically.

APPENDIX: DERIVATION OF TEM LINE SOURCE FIELDS IN A FDTD GRID

We present here a detailed derivation of the FDTD fields for open FDTD transmission lines. The four FDTD equations presented in equations (7)–(10) can be used to solve for the TEM FDTD fields. These equations lead to the dispersion and impedance relations for TEM waves which were previously derived for the closed transmission line fields. In addition, we employ here the two additional equations for e_z and h_z, which are

$$\begin{aligned}\frac{1}{\Delta}\eta_0 I_z^p(l,m,n) &= h_y^{p-1}(l,m,n) - h_y^{p-1}(l-1,m,n) \\ &\quad + h_x^{p-1}(l,m-1,n) - h_x^{p-1}(l,m,n) \qquad (55)\\ 0 &= e_x^p(l,m,n) - e_x^p(l,m+1,n) \\ &\quad + e_y^p(l+1,m,n) - e_y^p(l,m,n) \qquad (56)\end{aligned}$$

These equations in conjunction with the impedance relations determine the fields.

For the present problem the current I_z^p is given in Equation (38). As in the case of the TE excited line source [20], the solution here is found using the DFT to transform the FDTD difference equations to

algebraic equations. The DFT and IDFT pair is

$$H^x_{rsq}(n) = \sum_{lmp} h^p_x(l,m,n) e^{-2\pi i(rl+sm+qp)/N} \tag{57}$$

$$h^p_x(l,m,n) = \frac{1}{N^3} \sum_{rsq} H^x_{rsq}(n) e^{2\pi i(rl+sm+qp)/N} \tag{58}$$

Using the above transformation the current I^p_z becomes

$$\eta_0 I^z_{rsq}(n) = \eta_0 I_o N \delta_{(-q_o)q} e^{-2\pi i(rl_o+sm_o)/N + i\beta n\Delta} \tag{59}$$

where $q_o = Nk\Delta\tau/2\pi$ represents the source frequency [15]. Transforming the FDTD equations (7)–(10) and employing the above expression for the transformed current leads to a set of simultaneous equations in the transform domain which can be solved for the transformed electric and magnetic fields. The resulting solution is

$$H^x_{rsq}(n) = \frac{-\eta_0 I_o N \delta_{(-q_o)q} e^{-ik\Delta\tau + i\beta n\Delta}}{2i\Delta} \cdot \frac{e^{-2\pi i[rl_o + s(m_o - \frac{1}{2})]/N} \sin(\frac{\pi s}{N})}{\sin^2(\frac{\pi r}{N}) + \sin^2(\frac{\pi s}{N})} \tag{60}$$

$$H^y_{rsq}(n) = \frac{\eta_0 I_o N \delta_{(-q_o)q} e^{-ik\Delta\tau + i\beta n\Delta}}{2i\Delta} \cdot \frac{e^{-2\pi i[r(l_o - \frac{1}{2}) + sm_o]/N} \sin(\frac{\pi r}{N})}{\sin^2(\frac{\pi r}{N}) + \sin^2(\frac{\pi s}{N})} \tag{61}$$

for the magnetic fields in the transform domain. Applying the IDFT and taking the limit as the computational domain becomes infinite then gives the fields in the spatial domain, which are

$$h^p_x(l,m,n) = \frac{-\eta_0 I_o \Delta}{8i\pi^2} e^{-ik(p+1)\Delta\tau + i\beta n\Delta} \cdot \int_{-\frac{\pi}{\Delta}}^{\frac{\pi}{\Delta}} dk_x \int_{-\frac{\pi}{\Delta}}^{\frac{\pi}{\Delta}} dk_y \frac{\sin(\frac{k_y\Delta}{2}) e^{i[k_x(l-l_o) + k_y(m-m_o+\frac{1}{2})]\Delta}}{\sin^2(\frac{k_x\Delta}{2}) + \sin^2(\frac{k_y\Delta}{2})} \tag{62}$$

$$h^p_y(l,m,n) = \frac{\eta_0 I_o \Delta}{8i\pi^2} e^{-ik(p+1)\Delta\tau + i\beta n\Delta} \cdot \int_{-\frac{\pi}{\Delta}}^{\frac{\pi}{\Delta}} dk_x \int_{-\frac{\pi}{\Delta}}^{\frac{\pi}{\Delta}} dk_y \frac{\sin(\frac{k_x\Delta}{2}) e^{i[k_x(l-l_o+\frac{1}{2}) + k_y(m-m_o)]\Delta}}{\sin^2(\frac{k_x\Delta}{2}) + \sin^2(\frac{k_y\Delta}{2})} \tag{63}$$

One of the integrals in each of the above expressions can be evaluated using Cauchy's integral formula. The integrands have poles at

$$k_x = \pm k_{ox} \tag{64}$$

$$k_{ox} \equiv \frac{2i}{\Delta}\left|\sinh^{-1}\left[\sin\left(\frac{k_y\Delta}{2}\right)\right]\right| \tag{65}$$

$$\mathrm{Im}\{k_{ox}\} \geq 0 \tag{66}$$

The path can be closed as shown in Figure 13. For $l \geq l_o$ we close the path in the upper half plane, and for $l \leq l_o$ we close the path in the lower half plane. Notice that the value of the integrals along the paths at $k_x = \pm\pi/\Delta$ cancel each other due to the periodicity of the integrands. The value of the k_x integral in (62) is then $\pm 2\pi i R(\pm k_{ox})$ respectively for $l \geq l_o$ and $l \leq l_o$ where

$$\pm 2\pi i R(\pm k_{ox}) = \frac{2\sin(k_y\Delta/s)}{\Delta\sin(k_{ox}\Delta)} e^{i[k_{ox}|l-l_o|+k_y(m-m_o+\frac{1}{2})]\Delta} \tag{67}$$

The final solution for the x-component of the magnetic field is then given by

$$\begin{aligned} h_x^p(l,m,n) &= \frac{-\eta_0 I_o e^{-ik(p+1)\Delta\tau+i\beta n\Delta}}{2\pi} \\ &\quad \cdot \int_{-\frac{\pi}{\Delta}}^{\frac{\pi}{\Delta}} dk_y \frac{\sin(k_y\Delta/2)}{\sin(k_{ox}\Delta)} e^{i[k_{ox}|l-l_o|+k_y(m-m_o+\frac{1}{2})]\Delta} \qquad (68) \\ &= \frac{i\eta_0 I_o e^{-ik(p+1)\Delta\tau+i\beta n\Delta}}{4\pi} \\ &\quad \cdot \int_{-\frac{\pi}{\Delta}}^{\frac{\pi}{\Delta}} dk_y \frac{\mathrm{sgn}(k_y)}{\cos(k_{ox}\Delta/2)} e^{i[k_{ox}|l-l_o|+k_y(m-m_o+\frac{1}{2})]\Delta} \qquad (69) \end{aligned}$$

where we have used

$$\sin(k_{ox}\Delta/2) = i|\sin(k_y\Delta/2)| \tag{70}$$

Notice that for $l_o = m_o = 0$ the fields satisfy

$$h_y^p(l,m,n) = -h_x^p(m,l,n) \tag{71}$$

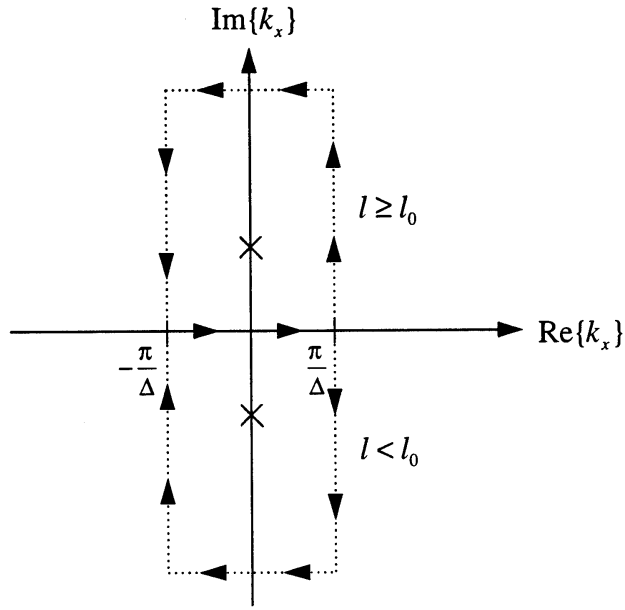

Figure 13. Contour in the complex k_x plane for evaluating the k_x integration. For $l \geq l_o$ the path is closed in the upper half plane; for $l < l_o$ the path is closed in the lower half plane. The horizontal paths are at infinity.

so that the y-component of the field can be determined from the x-component. This concludes the solution for the magnetic fields. As indicated above the electric fields are given directly in terms of the magnetic fields through the TEM wave impedance relations.

REFERENCES

1. Yee, K. S., "Numerical solution of initial boundary value problems involving maxwell's equations in isotropic media," *IEEE Trans. Anten. and Prop.*, Vol. AP-17, 585–589, 1966.
2. Taflove, A., and K. R. Umashankar, "The finite-difference time-domain method for numerical modeling of electromagnetic wave interactions with arbitrary structures," *PIER 2*, Ch. 8, Elsevier Science Publishing Co., Inc., 1990.

3. Shlager, K. L., and J. B. Schneider, "A selective survey of the finite-difference time-domain literature," *IEEE Antennas and Propagation Magazine*, Vol. 37, No. 4, 39–57, Aug. 1995.
4. Sheen, D. M., and S. M. Ali, "Application of the three-dimensional finite-difference time-domain method to the analysis of planar microstrip circuits," *IEEE Trans. on Microwave Theory and Techniques,* Vol. MTT-38, No. 7, 849–857, July 1990.
5. Yook, J. G., N. I. Dib, and L. P. B. Katehi, "Characterization of high frequency interconnects using the finite difference time domain and finite element methods," *IEEE Trans. on Microwave Theory and Techniques,* Vol. MTT-42, No. 9, 1727–1736, Sept. 1994.
6. Pillai, E., and W. Wiesbeck, "FDTD analysis of wideband aperture coupled interconnects," *Elect. Lett.*, Vol. 31, No. 12, 982–983, June 1995.
7. Harms, P. H., J. F. Lee, and R. Mittra,, "Characterizing the cylindrical via discontinuity," *IEEE Trans. on Microwave Theory and Techniques,* Vol. MTT-41, No. 1, 153–156, Jan. 1993.
8. Feix, N., M. Lalande, and B. Jecko, "Harmonic characterization of a microstrip bend via the finite difference time domain method," *IEEE Trans. on Microwave Theory and Techniqnes,* Vol. MTT-40, No. 5, 955–961, May 1992.
9. Moore, J., and H. Ling, "Characterization of a 90° microstrip bend with arbitrary miter via the time-domain finite difference method," *IEEE Trans. on Microwave Theory and Techniques,* Vol. MTT-38, No. 4, 1775–1787, April 1990.
10. Zhang, X., and K. K. Mei, "Time-domain finite difference approach to the calculation of the frequency-dependent characteristics of microstrip discontinuities," *IEEE Trans. on Microwave Theory and Techniques,* Vol. MTT-36, No. 12, 405–410, Dec. 1988.
11. Naishadham, K., and X. P. Lin, "Minimization of reflection error caused by absorbing boundary condition in the FDTD simulation of planar transmission lines," *IEEE Trans. on Microwave Theory and Techniques,* Vol. MTT-44, No. 1, 41–46, Jan. 1996.
12. Shorthouse, D. B., and C. J. Railton, "The incorporation of static field solution into the finite difference time domain algorithm," *IEEE Trans. on Microwave Theory and Techniques,* Vol. MTT-40, No. 5, 986–994, May 1992.
13. Railton, C. J., D. B. Shorthouse, and J. P. McGeehan, "Modeling of narrow microstrip lines using finite difference time domain method," *Elect. Lett.*, Vol. 28, No. 12, 1168–1170, June 1992.

14. Zhang, X., J. Y. Fang, K. K. Mei, and Y. Liu, "Calculations of the dispersive characteristics of microstrips by the time-domain finite difference method," *IEEE Trans. on Microwave Theory and Techniques*, Vol. MTT-36, No. 2, 263–267, Feb. 1988.
15. Oates, J. H., R. T. Shin, and M. J. Tsuk, "Small aperture modeling for EMI applications using the finite-difference time-domain technique," *J. Electromag. Waves and Appl.*, Vol. 9, No. 1/2, 37–69, 1995.
16. Oates, J. H., R. T. Shin, and M. J. Tsuk, "Modeling multiple interacting small apertures for EMI applications using the finite-difference time-domain technique," *Progress in Electromagnetic Research, PIER 12*, 75–105, 1996.
17. Fang, J., and D. Xeu, "Numerical errors in the computation of impedances by FDTD method and ways to eliminate them," *IEEE Microwave and Guided Wave Letters*, Vol. 5, No. 1, 6–8, Jan. 1995.
18. Chan, S. P., S. Y. Chan, and S. G. Chan, *Analysis of linear network and systems*, Addison-Wesley, Reading, MA, 1972.
19. Mittra, R., and T. Itoh, "Analysis of microstrip transmission lines," in *Advances in Microwaves,* 67–141, 1974, Academic Press, New York.
20. Oates, J. H., "Propagation and scattering of electromagnetic waves in complex environments," Ph.D. Dissertation, 1994, Department of Electrical Engineering and Computer Science, MIT.
21. Wheeler, H. A., "Transmission-line properties of a strip on a dielectric sheet on a plane," *IEEE Trans. on Microwave Theory and Techniques,* Vol. MTT-25, No. 8, 63.–647, Aug. 1977.
22. Wu, L. K., and Y. C. Chang, "Characterization of the shielding effects on the frequency-dependent effective dielectric constant of a waveguide-shielded microstrip using the finite-difference time-domain method," *IEEE Trans. on Microwave Theory and Techniques,* Vol. MTT-39, No. 10, 1688–1693, Oct. 1991.
23. Green, H. E., "The Numerical solution of transmission line problems," in *Advances in Microwaves*, 327–393, 1967, Academic Press, New York.